

# Localized numerical impulse solutions in diffuse neural networks modeled by the complex fractional Ginzburg-Landau equation

Alain Mvogo<sup>a,b,c,\*</sup>, Antoine Tambue<sup>d,e</sup>, Germain H. Ben-Bolie<sup>a,c</sup>, Timoléon C. Kofané<sup>a,c</sup>

<sup>a</sup>*Department of Physics, Faculty of Science, University of Yaounde I, P.O. Box 812, University of Yaounde, Cameroon*

<sup>b</sup>*The African Institute for Mathematical Sciences (AIMS), 6-8 Melrose Rd, Muizenberg 7945, South Africa*

<sup>c</sup>*Centre d'Excellence Africain en Technologies de l'Information et de la Communication, University of Yaounde I, Cameroon*

<sup>d</sup>*The African Institute for Mathematical Sciences (AIMS) and Stellenbosch University, 6-8 Melrose Road, Muizenberg 7945, South Africa*

<sup>e</sup>*Center for Research in Computational and Applied Mechanics (CERECAM), and Department of Mathematics and Applied Mathematics, University of Cape Town, 7701 Rondebosch, South Africa.*

---

## Abstract

We investigate localized wave solutions in a network of Hindmarsh-Rose neural model taking into account the long-range diffusive couplings. We show by a specific analytical technique that the model equations in the infrared limit (wave number  $k \rightarrow 0$ ) can be governed by the complex fractional Ginzburg-Landau (CFGL) equation. According to the stiffness of the system, we propose both the semi and the linearly implicit Riesz fractional finite-difference schemes to solve efficiently the CFGL equation. The ob-

---

\*Corresponding author

*Email addresses:* [mvogo@aims.ac.za](mailto:mvogo@aims.ac.za) (Alain Mvogo), [antonio@aims.ac.za](mailto:antonio@aims.ac.za) (Antoine Tambue), [gbenbolie@yahoo.fr](mailto:gbenbolie@yahoo.fr) (Germain H. Ben-Bolie), [tckofane@yahoo.com](mailto:tckofane@yahoo.com) (Timoléon C. Kofané)

tained fractional numerical solutions for the nerve impulse reveal localized short impulse properties. We also show the equivalence between the continuous CFGL and the discrete Hindmarsh-Rose models for relatively large network.

*Keywords:* Localized solutions, Hindmarsh-Rose neural model, complex fractional Ginzburg-Landau equation, Riesz fractional finite-difference schemes.

---

## 1. Introduction

The interest in investigating and controlling the propagation of waves in neural tissues has been increasingly growing during the last decades. This is because the conditions under which cortical waves occur are very primordial in the understanding of the normal processing of sensory stimuli as well as more pathological forms of behavior [1, 2]. In that sense, many studies have been carried out that indicated the presence of localized nonlinear waves in the neural systems (see, e.g., [3] and references therein). Interestingly, the recent work by Kakmeni *et al.* reported on the presence of these waves of the nerve impulse in diffusive Hindmarsh-Rose (HR) neural networks with nearest-neighbor couplings [3]. Also, as recently demonstrated, the dynamics of an individual neuron in diffusive HR neural networks may be influenced by the interaction or coupling with other neurons [4, 5]. It would be interesting now to see what are the effects that the long-range diffusive coupling or interaction has on the wave propagation in such a network.

The intuitively obvious fact that many biological systems are systems with

memory or aftereffects is now confirmed by many researches. The modeling of these systems by fractional-order differential equations has more advantages than the classical mathematical modeling using the integer-order, in which such effects are neglected. As it has been shown, even processing of external stimuli by individual neural oscillator can be described by fractional differentiation [6, 7]. In many cases memory effect obeys the power law and the corresponding system could be described by fractional differential equation. It becomes also now interesting to investigate localized waves in such an equation in diffusive neural networks when the long-range coupling is taken into account.

We aim in this paper to study the properties of localized waves in the diffusive HR neural networks with long-range interactions that can work in some way as a long memory. We show that the model can be governed in the infrared limit (wave number  $k \rightarrow 0$ ) can be governed by the complex fractional Ginzburg-Landau (CFGL) equation. According to the stiffness of the system, we propose both the semi and the linearly implicit Riesz fractional finite-difference schemes to solve efficiently the CFGL equation. The obtained fractional numerical solutions for the nerve impulse reveal localized short impulse properties. The fractional order mostly contributes to the behavior of the tails of the impulse. It is also shown the equivalence between the continuous CFGL and the discrete Hindmarsh-Rose models for relatively large network.

The rest of the paper is organized as follows. In Section 2, we present the neural network taking into account the long-range diffusive coupling. In Section 3, by means of the perturbation technique, we derive the complex

fractional Ginzburg-Landau (CFGL) equation which describes the equation of motion. In Section 4, we solve efficiently the CFGL equation following closely [8] in space discretization, and propose the semi-implicit Riesz fractional finite-difference scheme and the linearly implicit Riesz fractional finite-difference scheme where only one linear system is solved by time iteration. We then present the numerical results and show the equivalence between the continuous CFGL model and the discrete HR model for relatively large network. Our work is summarized in Section 5.

## 2. The Hindmarsh-Rose coupled model

Many nontrivial examples of dynamical systems have been provided by phenomenological and neurophysiological models developed to reproduce the activities of neural oscillators. The Hindmarsh-Rose model [9], a generalization of the Fitzhugh equations [10], represents a paradigmatic example of these systems. It aims to study the spiking-bursting behavior of the membrane potential observed in the single neuron experiments. In this paper, following Refs. [3, 4] we generalize the HR neural model assuming only that the coupling between neural oscillators are long-ranged through the membrane potential variable. The HR neural network is then assumed as a system of  $N$  neural oscillators in which the configuration of couplings is assumed to be power long-ranged. In this case, each unit of HR neural model is coupled to any other. The model can be reformulated by means of the following nonlinear ordinary differential equations:

$$\begin{cases} \dot{u}_n = v_n - au_n^3 + bu_n^2 - w_n + I + \sum_{m=1, m \neq n}^N K_\alpha(n-m)(u_n - u_m), \\ \dot{v}_n = c - du_n^2 - ev_n, \\ \dot{w}_n = r[s(u_n - u_0) - w_n], \end{cases} \quad (1)$$

where the variable  $u$  is the membrane potential (nerve impulse),  $v$  is the spiking variable which takes into account the measure of the rate at which transport of sodium and potassium ions is made through fast ion channels, and  $w$  is the bursting variable which takes into account the rate at which the transport of other ions ( $Cl^-$  and proteins anions) made through slow ions channels. The values of the parameters of the HR model are  $a = 1.0$ ,  $b = 3.0$ ,  $c = 1.0$ ,  $d = 5.0$ ,  $r = 0.008$ ,  $s = 4.0$ ,  $e = 1.0$ ,  $u_0 = -1.60$  and  $2.92 < I < 3.40$ .

Physiologically, responses generated within the cell can travel not only to neighboring cells through intercellular communication using a gap-junction but also through extracellular communication, involving the secretion of molecular signals such as neurotransmitters. Then, in comparison to the model of Ref. [3], the present HR model is generalized via the presence of the term  $\sum_{m \neq n} K_\alpha(m-n)(u_n - u_m)$  which characterizes long-range diffusive interaction in the system and can appear as an effective interaction in dispersive and complex systems [11, 12, 13]. The latter is due to the fact that the extracellular messenger can propagate from one cell to its direct neighbors and even extend to other neighboring non-contacting cells. The nonlocal coupling interaction is given by the power-law dependence

$$K_\alpha(n) = \frac{K}{|n|^{\alpha+1}}, \quad (2)$$

where  $K$  is the coupling parameter such as the synaptic strength, while  $\alpha$  which is the LRI parameter, physically describes a level of collective interaction of neural oscillators.

It has been demonstrated by Steur *et al.* [5] that such a neural system (1) coupled via diffusive coupling is semi-passive, then the solutions of all connected systems in the network are bounded. We are interested by non-linear waves in the network. To achieve this, we first differentiate the first equation of (1) and substitute  $\dot{v}_n$  into the obtained second-order ordinary differential equation. Then, we rewrite suitably (1) in a Lienard form, that is a second-order differential equation with a small damping term, such that

$$\left\{ \begin{array}{l} \ddot{u}_n + \Omega_0^2 u_n + (\eta_0 + \eta_1 u_n + \eta_2 u_n^2) \dot{u}_n + \lambda_1 u_n^2 + \frac{\eta_2}{3} u_n^3 + \lambda_3 w_n + I_0 \\ \quad = \sum_{m=1, m \neq n}^N \frac{1}{|n-m|^{\alpha+1}} [c_0(u_n - u_m) + c_1(\dot{u}_n - \dot{u}_m)] \\ \dot{v}_n = c - d u_n^2 - e v_n \\ \dot{w}_n = r[s(u_n - u_0) - w_n], \end{array} \right. \quad (3)$$

where  $\Omega_0$ ,  $\eta_0$ ,  $\eta_1$ ,  $\eta_2$ ,  $\lambda_1$ ,  $\lambda_3$ ,  $I_0$ ,  $c_0$  and  $c_1$  are constant parameters related to those of (1) such as  $\Omega_0^2 = rs$ ,  $\eta_0 = e$ ,  $\eta_1 = 2b$ ,  $\eta_2 = 3ea$ ,  $\lambda_1 = d - eb$ ,  $\lambda_3 = e - r$ ,  $I_0 = c + rsu_0 + I$ ,  $c_0 = eK$  and  $c_1 = K$ . In general, the solutions of (3) can be obtained using perturbation techniques. In that sense, we introduce the following variables  $u_n = \varepsilon \psi_n$ ,  $v_n = \varepsilon \Phi_n$  and  $w_n = \varepsilon \beta_n$ , where  $\varepsilon \ll 1$ . By keeping in the development the first two nonlinear terms, the governing equations of motion in the neural network then become

$$\left\{ \begin{array}{l} \ddot{\psi}_n + \Omega_0^2 \psi_n + \varepsilon(\varepsilon\eta_0 + \eta_1 \psi_n + \varepsilon\eta_2 \psi_n^2) \dot{\psi}_n + \varepsilon\lambda_1 \psi_n^2 + \varepsilon^2 \frac{\eta_2}{3} \psi_n^3 + \varepsilon^2 \lambda_3 \beta_n \\ \quad = \sum_{m=1, m \neq n}^N \frac{1}{|n-m|^{\alpha+1}} \left[ c_0(\psi_n - \psi_m) + \varepsilon^2 c_1(\dot{\psi}_n - \dot{\psi}_m) \right] \\ \dot{\Phi}_n + \varepsilon d \psi_n^2 + e \Phi_n = 0 \\ \dot{\beta}_n + r \beta_n - \Omega_0^2 \psi_n = 0. \end{array} \right. \quad (4)$$

While writing (4), the coupling parameter  $\lambda_3$  of the membrane potential with the bursting variable has been perturbed of order  $\varepsilon^2$ , taking into account the fact that the variation of the bursting variable is slower than the one of the membrane potential. In addition, as we are interested by an analysis in a weakly dissipative medium, we have assumed the parameters  $\eta_0$  and  $c_1$  to be perturbed at the order  $\varepsilon^2$ .

### 3. Equation of motion

The chain of the neural network is a very long having several thousand neural oscillators compared to the distance between the neighboring neural oscillators along the chain. It is therefore appropriate to make a continuum approximation, which is also valid in the long wavelength limit. The non-locality features of the medium often impose the necessity of using non-traditional tools. In that follows, we first assume for Eq. (4) the following solutions

$$\left\{ \begin{array}{l} \psi_n = \varepsilon(B_n^{(1)} e^{i\theta_n} + c.c) + \varepsilon^2[C_n^{(1)} + (D_n^{(1)} e^{2i\theta_n} + c.c)] \\ \Phi_n = \varepsilon(B_n^{(2)} e^{i\theta_n} + c.c) + \varepsilon^2[C_n^{(2)} + (D_n^{(2)} e^{2i\theta_n} + c.c)] \\ \beta_n = \varepsilon(B_n^{(3)} e^{i\theta_n} + c.c) + \varepsilon^2[C_n^{(3)} + (D_n^{(3)} e^{2i\theta_n} + c.c)], \end{array} \right. \quad (5)$$

with  $\theta_n = kn - \Omega t$ , where  $k$  is the normal mode wave vector and  $\Omega$  is the angular velocity of the wave. The variable  $t$  is rescaled through the perturbative small parameter  $\varepsilon$  as  $t \rightarrow \varepsilon^2 t$ .

In the following, we replace the solutions (5) and their derivatives in the new membrane potential equation of motion given by the first equation of (4). We then group the terms in the same power of  $\varepsilon$ , which leads us to a system of equations. Each of these equations will correspond to each approximation for specific harmonics. To reach this goal, we consider the infinite network of neural oscillators ( $N \rightarrow \infty$ ). We multiply Eq. (4) by  $\exp(-ikn)$  and we sum over  $n$  from  $-\infty$  to  $+\infty$ . Then, we introduce the following functions

$$\left\{ \begin{array}{l} f^j(k, t) = \sum_{n=-\infty}^{\infty} e^{-ikn} B_n^{(j)}(t) \\ g^j(k, t) = \sum_{n=-\infty}^{\infty} e^{-ikn} C_n^{(j)}(t) \\ h^j(k, t) = \sum_{n=-\infty}^{\infty} e^{-ikn} D_n^{(j)}(t) \\ \tilde{J}_\alpha(k) = \sum_{n=-\infty}^{\infty} e^{-ikn} \frac{1}{|n|^{\alpha+1}}, \end{array} \right. \quad (6)$$

with  $j = 1, 2, 3$ , and

$$\tilde{J}_\alpha(0) = 2 \sum_{n=1}^{\infty} \frac{1}{|n|^{\alpha+1}} = 2\zeta(\alpha + 1),$$

where  $\zeta(\alpha)$  is the Riemann zeta function.

In the long-wave limit, we may adopt  $f^j(k, t)$ ,  $g^j(k, t)$  and  $h^j(k, t)$  as  $k^{th}$  Fourier components of continuous functions  $B^{(j)}(x, t)$ ,  $C^{(j)}(x, t)$  and  $D^{(j)}(x, t)$ , respectively such that  $B_n^{(j)}(t) \rightarrow B^{(j)}(x, t)$ ,  $C_n^{(j)}(t) \rightarrow C^{(j)}(x, t)$  and  $D_n^{(j)}(t) \rightarrow D^{(j)}(x, t)$ . The functions are related each other by the Fourier transforms such that

$$\begin{cases} B^{(j)}(x, t) = \frac{1}{2\pi} \int_{-\infty}^{\infty} e^{ikx} f^j(k, t) dk \\ C^{(j)}(x, t) = \frac{1}{2\pi} \int_{-\infty}^{\infty} e^{ikx} g^j(k, t) dk \\ D^{(j)}(x, t) = \frac{1}{2\pi} \int_{-\infty}^{\infty} e^{ikx} h^j(k, t) dk. \end{cases} \quad (7)$$

After some algebras, at the order  $\varepsilon^1$  after the annihilation of terms in  $e^{\pm i\theta}$ , we obtain the relation

$$\Omega^2 = \Omega_0^2 + c_0 a_\alpha |k|^\alpha, \quad (8)$$

which determines the dispersion relation of linear waves of the system. As displayed in Figure 1, the corresponding linear spectrum is reduced when  $\alpha$  increases. To obtain (8), we have used the infrared approximation [14, 16]

$$[\tilde{J}_\alpha(0) - \tilde{J}_\alpha(k)] \approx a_\alpha |k|^\alpha, \quad (0 < \alpha < 2, \alpha \neq 1) \quad (9)$$

where  $a_\alpha = 2\Gamma(-\alpha) \cos(\pi\alpha/2)$ .

At the order  $\varepsilon^2$ , terms without exponential dependence give

$$C^{(1)} = -\frac{2\lambda_1}{\Omega_0^2} |B^{(1)}|^2, \quad (10)$$

while at the same order, terms with  $e^{2i\theta}$  give the relation

$$D^{(1)} = \frac{\lambda_1 - i\Omega\eta_1}{\Omega_1^2} (B^{(1)})^2. \quad (11)$$

where  $\Omega_1^2 = 2\Omega_0^2 + \Omega^2 + 4(\Omega^2 - \Omega_0^2)^2$ .

For the third equation of (3), at the order  $\varepsilon^1$  the terms with  $e^{i\theta}$  give the relation

$$B^{(3)} = \frac{\Omega_0^2(r + i\Omega)B^{(1)}}{r^2 + \Omega^2}. \quad (12)$$

Collecting all the terms depending on  $e^{i\theta}$  in (4) at the order  $\varepsilon^3$ , we obtain the following equation

$$\begin{aligned} -2i\Omega \frac{\partial B^{(1)}}{\partial t} = & i\Omega\eta_0 B^{(1)} + (i\Omega\eta_1 - 2\lambda_1)(B^{(1)}C^{(1)} + B^{(1*)}D^{(1)}) \\ & + (i\Omega - 1)\eta_2 |B^{(1)}|^2 B^{(1)} - \lambda_3 \frac{\Omega_0^2(r + i\Omega)}{r^2 + \Omega^2} B^{(1)} \\ & - ic_1\Omega(a_\alpha |k|^\alpha B^{(1)}). \end{aligned} \quad (13)$$

Rewriting this equation taking into account the connection between the Riesz fractional derivative and its Fourier transform [17]

$$|k|^\alpha \longleftrightarrow -\frac{\partial^\alpha}{\partial |x|^\alpha}, \quad |k|^2 \longleftrightarrow -\frac{\partial^2}{\partial |x|^2} \quad (14)$$

we obtain

$$\frac{\partial B^{(1)}}{\partial t} = \gamma B^{(1)} + P_r \frac{\partial^\alpha B^{(1)}}{\partial |x|^\alpha} - Q |B^{(1)}|^2 B^{(1)}, \quad (15)$$

where the coefficients  $\gamma$ ,  $P_r$  and  $Q$  are given by

$$\gamma = \gamma_r + i\gamma_i, \quad P_r = c_1 a_\alpha / 2 \quad \text{and} \quad Q = Q_r + iQ_i.$$

The coefficients  $\gamma_r$  and  $\gamma_i$  are the real and imaginary parts of the dissipation coefficient. For the nonlinearity coefficient the same terminology is used. The coefficients  $Q_r$ ,  $Q_i$ ,  $\gamma_r$  and  $\gamma_i$  are given by

$$\begin{aligned} \gamma_r = & \frac{\lambda_3 \Omega_0^2}{2(r^2 + \Omega^2)} - \frac{\eta_0}{2}, \quad \gamma_i = -\frac{r \lambda_3 \Omega_0^2}{2\Omega(r^2 + \Omega^2)}, \\ Q_r = & \frac{\eta_2}{2} - \frac{\eta_1 \lambda_1}{\Omega_0^2} + \frac{3\eta_1 \lambda_1}{2\Omega_1^2}, \quad Q_i = \frac{1}{\Omega} \left( \frac{\eta_2}{2} - \frac{\Omega^2 \eta_1^2 - 2\lambda_1^2}{2\Omega_1^2} - \frac{2\lambda_1^2}{\Omega_0^2} \right). \end{aligned}$$

Equation (15) which is a new general theoretical framework derived in our neural network is the complex fractional Ginzburg-Landau equation. This confirms the fact that the brain may actively work effectively using the spatial dimension for information processing but not only in time domain [20, 21, 22]. In Ref. [15], the fractional Ginzburg-Landau equation is derived from the variational Euler Lagrange equation for fractal media. In the present work, we confirm once more the fact that using the Fourier transforms and the infrared limit, the long-range interactions lead under special conditions to the fractional dynamics [14, 16, 17]. The fractional Ginzburg-Landau equation has been proposed by Weitzner and Zaslavsky [18] to describe the dynamical processes in a medium with fractal dispersion. Its generalization has been used by Milovanov and Rasmussen [19] as an unconventional approach to critical phenomena in complex media.

In this work, the motion of modulated waves in diffuse neural networks are proven to be described by the CFGL equation. The infrared limit of an infinite chain of neural oscillators with the long-range diffusive interactions can be described by equations with the fractional Riesz coordinate derivative of order  $\alpha < 2$ . To the best of our knowledge, this is the first research work that attempts to describe the dynamical behavior of neural networks with an equation of fractional order. This result suggests that neurons can participate in a collective processing of long-scale information, a relevant part of which is shared over all neurons.

#### 4. The Semi-implicit Riesz fractional finite-difference and the linearly Riesz fractional finite-difference schemes

In the previous section, we have demonstrated that the HR neural network can be elegantly described by the CFGL equation. In general, analytical and closed solutions of fractional equations cannot be obtained. In that case, numerical techniques are used to identify the solution behavior of such fractional equations. In this section, we provide the semi-implicit Riesz fractional finite-difference scheme and the linearly implicit Riesz fractional finite-difference scheme to find numerically localized wave solutions for the CFGL equation (11). We also show numerically the equivalent between the continuous CFGL model and the discrete HR model for relatively large network.

To begin our numerical analysis, it is convenient to recall the CFGL equation (15) as

$$\begin{cases} \frac{\partial B^1}{\partial t} = P_r \frac{\partial^\alpha B^1}{\partial |x|^\alpha} + (\gamma_r + i\gamma_i)B^1 - (Q_r + iQ_i)|B^1|^2 B^1, \\ B^1(x, 0) = g(x), \quad x \in [0, b_0], \\ B^1(0, t) = \phi_1(t), \quad B^1(b_0, t) = \phi_2(t), \quad t \in (0, T], \end{cases} \quad (16)$$

The functions  $g, \phi_1$  and  $\phi_2$  are sufficiently smooth functions. Note that  $B^1 \equiv B^{(1)}$ , the function  $g$  is the initial solution,  $T > 0$  is the final time and  $\frac{\partial^\alpha}{\partial |x|^\alpha}$  is space Riesz fractional derivative of order  $\alpha$  given for  $0 < \alpha < 2$ ,  $\alpha \neq 1$  by

$$\frac{\partial^\alpha}{\partial |x|^\alpha} = -c_\alpha \left( -\infty D_x^\alpha + {}_x D_{+\infty}^\alpha \right), \quad (17)$$

where the coefficient

$$\begin{cases} c_\alpha = \frac{1}{2 \cos(\alpha\pi/2)}, \\ {}_{-\infty}D_x^\alpha B^1 = \left(\frac{d}{dx}\right)^m [{}_{\infty}I_x^{m-\alpha} B^1(x, t)], \\ {}_x D_{+\infty}^\alpha B^1 = (-1)^m \left(\frac{d}{dx}\right)^m [{}_x I_{+\infty}^{m-\alpha} B^1(x, t)], \end{cases} \quad (18)$$

with  $m \in \mathbb{N}$  such that  $m - 1 < \alpha \leq m$ . The terms  ${}_{-\infty}D_x^\alpha$  and  ${}_x D_{+\infty}^\alpha$  are respectively the left and the right side Riemann-Liouville fractional derivatives.

The left and right side Weyl fractional integrals used in (18) are defined by

$$\begin{cases} {}_{\infty}I_x^{m-\alpha} B^1(x, t) = \frac{1}{\Gamma(\alpha)} \int_{-\infty}^x (x - \zeta)^{\alpha-1} B^1(\zeta, t) d\zeta, \\ {}_x I_{+\infty}^{m-\alpha} B^1(x, t) = \frac{1}{\Gamma(\alpha)} \int_x^{+\infty} (x - \zeta)^{\alpha-1} B^1(\zeta, t) d\zeta. \end{cases} \quad (19)$$

By setting  $B^1 = U + iV$ , where  $U$  and  $V$  are respectively the real and imaginary parts of  $B^1$ , (16) is equivalent to the following coupled system

$$\begin{cases} \frac{\partial U}{\partial t} = P_r \frac{\partial^\alpha U}{\partial |x|^\alpha} + \gamma_r U - \gamma_i V - (Q_r U - Q_i V)(U^2 + V^2), \\ \frac{\partial V}{\partial t} = P_r \frac{\partial^\alpha V}{\partial |x|^\alpha} + \gamma_i U + \gamma_r V - (Q_i U + Q_r V)(U^2 + V^2), \\ U(x, 0), V(x, 0) = g(x), \quad x \in [0, b_0], \\ U(0, t) = \text{Re}(\phi_1(t)), U(b_0, t) = \text{Re}(\phi_2(t)), \\ V(0, t) = \text{Im}(\phi_1(t)), V(b_0, t) = \text{Im}(\phi_2(t)), \quad t \in (0, T], \end{cases} \quad (20)$$

where  $\text{Re}$  and  $\text{Im}$  are respectively the real part and the imaginary part. Let us use the following identification  $B^1 \equiv (U, V)^T$ . By setting

$$\mathcal{A} = \begin{pmatrix} P_r \frac{\partial^\alpha}{\partial |x|^\alpha} + \gamma_r & -\gamma_i \\ \gamma_i & P_r \frac{\partial^\alpha}{\partial |x|^\alpha} + \gamma_r \end{pmatrix}, \quad (21)$$

$$F_1(B^1) = \begin{pmatrix} -(Q_r U - Q_i V)(U^2 + V^2) \\ -(Q_i U + Q_r V)(U^2 + V^2) \end{pmatrix}, \quad (22)$$

the coupled system (20) becomes

$$\begin{cases} \frac{\partial B^1}{\partial t} = \mathcal{A}B^1 + F_1(B^1), \\ B^1(x, 0) = g(x), \quad x \in [0, b_0], \\ B^1(0, t) = \phi_1(t), B^1(b_0, t) = \phi_2(t). \end{cases} \quad (23)$$

For space discretization, we use the weighted Riesz fractional finite-difference approximation as presented in [8, 30]. We divide the interval  $(0, b_0)$  into  $M$  sub-interval with the step  $h = b_0/M$ . In order to perform the space discretization with our homogeneous boundary conditions, the function  $B^1$  should be extended to the whole  $\mathbb{R}$  (see [8]) as

$$B_*^1(x, t) \equiv (U^*, V^*)^T = \begin{cases} B^1(x, t), & x \in [0, b_0], \\ (0, 0)^T, & x \in (-\infty, 0) \cup (b_0, +\infty). \end{cases} \quad (24)$$

Using (24), each component of the function  $B^1$  can be discretized by the centered finite difference as follows for  $0 < \alpha < 2$ ,  $\alpha \neq 1$

$$\frac{\partial^\alpha B_*^1}{\partial |x|^\alpha} = \begin{pmatrix} -\frac{1}{h^\alpha} \sum_{-\infty}^{+\infty} w_k^\alpha U^*(x-kh, t) + \mathcal{O}(h^2) \\ -\frac{1}{h^\alpha} \sum_{-\infty}^{+\infty} w_k^\alpha V^*(x-kh, t) + \mathcal{O}(h^2) \end{pmatrix}. \quad (25)$$

Since  $B_*^1(x, t) = (0, 0)^T$  for  $x \in (-\infty, 0) \cup (b_0, +\infty)$ , we therefore have

$$\frac{\partial^\alpha B^1}{\partial |x|^\alpha} = \begin{pmatrix} -\frac{1}{h^\alpha} \sum_{-(b_0-x)/h}^{(x-0)/h} w_k^\alpha U(x-kh, t) + \mathcal{O}(h^2) \\ -\frac{1}{h^\alpha} \sum_{-(b_0-x)/h}^{(x-0)/h} w_k^\alpha V(x-kh, t) + \mathcal{O}(h^2) \end{pmatrix}. \quad (26)$$

where

$$w_k^\alpha = \frac{(-1)^k \Gamma(\alpha + 1)}{\Gamma(\alpha/2 - k + 1) \Gamma(\alpha/2 + k + 1)}. \quad (27)$$

Denote by  $U_i^h(t)$  and  $V_i^h(t)$  the approximated values of  $U(x_i, t)$  and  $V(x_i, t)$  respectively, the central finite difference approximation is therefore given by

$$\frac{\partial^\alpha B^1(x_i, t)}{\partial |x|^\alpha} \approx \begin{pmatrix} -\frac{1}{h^\alpha} \sum_{k=-M+i}^i w_k^\alpha U_{i-k}^h(t) \\ -\frac{1}{h^\alpha} \sum_{k=-M+i}^i w_k^\alpha V_{i-k}^h(t) \end{pmatrix}, i = 1, \dots, M-1. \quad (28)$$

Note that  $U_0^h(t) = \text{Re}(\phi_1(t))$ ,  $U_M^h(t) = \text{Re}(\phi_2(t))$ ,  $V_0^h(t) = \text{Im}(\phi_1(t))$  and  $V_M^h(t) = \text{Im}(\phi_2(t))$ . By setting  $U_h = (U_i^h)_{1 \leq i \leq M-1}$ ,  $V_h = (V_i^h)_{1 \leq i \leq M-1}$  and  $B_h^1 = (U_h, V_h)^T$ , the semi discrete version of (23) after space discretization is given by

$$\begin{cases} \frac{dB_h^1}{dt} = \mathcal{A}_h B_h^1 + F(B_h^1), \\ B_h^1(0) = (g(x_i))_{1 \leq i \leq M-1}. \end{cases} \quad (29)$$

where

$$\mathcal{A}_h = \begin{pmatrix} -\mathbf{P} + \gamma_r \mathbf{I} & -\gamma_i \mathbf{I} \\ \gamma_i \mathbf{I} & -\mathbf{P} + \gamma_r \mathbf{I} \end{pmatrix}, \quad (30)$$

$$\mathbf{P} = (p_{ij})_{1 \leq i, j \leq M-1}, \quad p_{ij} = \frac{Pr}{h^\alpha} w_{i-j}^\alpha, \quad F(B_h^1) = F_1(B_h^1) + Bc(t), \quad (31)$$

$Bc(t)$  being the contribution of the Dirichlet boundary condition, which should be expressed as a function of  $\phi_1(t)$  and  $\phi_2(t)$ . Note that  $\mathbf{I}$  is the  $(M-1) \times (M-1)$  identity matrix. Please also note that the matrix  $\mathcal{A}_h$  is more than 50 % full.

Let  $N$  being the time subdivision, we use the constant time step  $\tau = T/N$ . In order to fully discretize (23), let  $B_{h,n}^1$  being our approximated solution of  $B^1(n\tau) = (B^1(x_i, n\tau))_{1 \leq i \leq M-1}$ . From (29), the  $\theta$ - Euler Riesz fractional finite-difference scheme to approximate (23) is given by

$$\frac{B_{h,n+1}^1 - B_{h,n}^1}{\tau} = \theta (\mathcal{A}_h B_{h,n}^1 + F(B_{h,n}^1)) + (1 - \theta) (\mathcal{A}_h B_{h,n+1}^1 + F(B_{h,n+1}^1)) \quad (32)$$

$$0 \leq \theta \leq 1.$$

For  $\theta = 1$ , the scheme is an explicit Riesz fractional finite-difference scheme, while for  $\theta = 0$ , the scheme is a fully implicit Riesz fractional finite-difference scheme. The high order accuracy in time is obtained for  $\theta = \frac{1}{2}$ , which corresponds to the Crank-Nicholson Riesz fractional finite-difference approximation scheme. Note the for  $\theta = 0$ , the corresponding explicit scheme is only stable for very small time step  $\tau$ . For  $\theta \neq 1$ , the scheme is more stable, but the fact that the matrix  $\mathcal{A}_h$  is likely to be more than 50 % full (depending of the sparseness of  $\mathbf{P}$ ) makes the Newton iterations less efficient. High order implicit Runge-kutta methods can be used if high order accuracy is needed, but these methods will be extremely less efficient.

To solve the efficiency drawback of the implicit schemes, we propose in this work two simple schemes.

For nonstiff nonlinear part  $F$ , we consider the semi-implicit Riesz fractional finite-difference scheme where the linear part of (29) is approximated implicitly and the nonlinear part explicitly. Following [23, 24, 25], the corresponding scheme is given by

$$\frac{B_{h,n+1}^1 - B_{h,n}^1}{\tau} = \mathcal{A}_h B_{h,n+1}^1 + F(B_{h,n}^1). \quad (33)$$

For stiff nonlinear part  $F$ , scheme (33) will require small time steps to be stable, following [29] we consider the following the linearly implicit Riesz fractional finite-difference scheme given by

$$B_{h,n+1}^1 = B_{h,n}^1 + \tau (\mathbf{I} - \tau J_n)^{-1} (\mathcal{A}_h B_{h,n}^1 + F(B_{h,n}^1)), \quad (34)$$

$$J_n = \mathcal{A}_h + \partial_{B^1} F(B_{h,n}^1). \quad (35)$$

Obviously the semi-implicit scheme given at (33) and the linearly implicit

Riesz fractional finite-difference scheme are very efficient than the implicit schemes given in (32) for  $\theta \neq 1$ , as only one linear system is solved per time iteration.

Following again [29], we can also obtain the  $s$ -stages Rosenbrock Riesz fractional finite-difference schemes if high order accuracy is needed. Such schemes will be efficient as only  $s$  linear systems are required by time iteration.

#### 4.1. Numerical results

##### 4.1.1. Numerical simulations of the CFGL equation and localized wave solutions

Numerical simulations of (15) are performed using the the linearly implicit Riesz fractional finite-difference scheme given by (34) as the nonlinear function  $F$  is stiff. We choose the solution of  $B^1(x, 0)$  in the form of a nonlinear solution of the standard complex Ginzburg Landau equation [26, 27]

$$B^1(x, 0) = \frac{B_0 e^\theta}{1 + e^{(\theta + \theta^*)(1 + i\mu)}}, \quad \phi_1(t) = \phi_2(t) = 0, \quad t \in (0, T]. \quad (36)$$

where the real part and the imaginary part of  $B^1(x, 0)$  are given respectively by

$$\begin{cases} B_r^1(x, 0) = U(x, 0) = B_0 \left[ \frac{e^{-\theta} + \cos(2\mu\theta)e^\theta}{2(\cosh(2\theta) + \cos(2\mu\theta))} \right], \\ B_i^1(x, 0) = V(x, 0) = -B_0 \left[ \frac{\sin(2\mu\theta)e^\theta}{2(\cosh(2\theta) + \cos(2\mu\theta))} \right], \end{cases} \quad (37)$$

where  $\theta = kx$ ,  $\mu = -\beta + \sqrt{2 + \beta^2}$  and  $\beta = -\frac{3Q_r}{2Q_i}$ .

The parameter values are:  $\Omega_0^2 = 0.032$ ,  $k = 1.5$ ,  $I = 3$ ,  $\lambda_1 = 2$ ,  $\lambda_3 = 0.992$ ,  $\eta_0 = 1$ ,  $\eta_1 = 6$ ,  $\eta_2 = 3$ ,  $r = 0.008$ ,  $c_0 = 0.001$ ,  $c_1 = 0.001$  and  $B_0 = 0.5$ .

Figure 2 displays the spatiotemporal evolution on the amplitude for  $\alpha = 1.8$  at time  $t = 0.001$ . We observe in this figure that the solution is well localized nonlinear excitation in space and time, it has the shape of a short pulse and propagates without any change of its profile. It is clear from there that as time evolves, the form of the pulse does not change; it is structurally stable.

Figure 3 displays spatial profiles of the amplitude of the solution for three distinct values of parameter  $\alpha$ , namely  $\alpha = 1.7$ ,  $\alpha = 1.8$  and  $\alpha = 1.92$  for the time instant  $t = 0.001$ . We observe in the graphs of Figure 3 that the solution is well localized in space with the shape of a short pulse and its amplitude decreases with the increasing of  $\alpha$ . Then, The fractional order mostly contributes to the behavior of the tails of the short pulse numerical solutions. Remarkably, the pulse profiles in Figure 3 are in qualitative agreement with the typical results reported in electrodynamics theory in both myelinated and myelin-free nerve fiber contexts [28].

#### *4.1.2. Reconstruction of the discrete solutions from continuous CFGL solution*

In order to check the validity of our fractional approach and to get an idea of what kind of dynamical waves one might obtain in the neural network, we carried out numerical simulation of (1) and compare the results with the one of the fractional model (16). The simulation of (1) is performed through the fourth-order Runge-Kutta scheme.

Remember that

$$B^1(x, t) = B_r^{(1)}(x, t) + iB_i^{(1)}(x, t) = U(x, t) + iV(x, t).$$

From the first equation of (5), we have

$$\psi = 2\varepsilon(B_r^{(1)} \cos \theta - B_i^{(1)} \sin \theta) + \varepsilon^2[C^{(1)} + 2(D_r^{(1)} \cos 2\theta - D_i^{(1)} \sin 2\theta)], \quad (38)$$

where  $\theta = kx - \Omega t$ ,  $D_r^{(1)}$  and  $D_i^{(1)}$  are the real and imaginary parts of  $D^{(1)}$ .

From (11) we have

$$D^{(1)} = (a_1 - ia_2)[B^1]^2, \quad a_1 = \frac{\lambda_1}{\Omega_1^2}, \quad a_2 = \frac{\Omega\eta_1}{\Omega_1^2}, \quad (39)$$

which leads to

$$D_r^{(1)}(x, t) = a_1(B_r^{(1)2} - B_i^{(1)2}) + 2a_2B_r^{(1)}B_i^{(1)}, \quad (40)$$

$$D_i^{(1)}(x, t) = a_2(B_i^{(1)2} - B_r^{(1)2}) + 2a_1B_r^{(1)}B_i^{(1)}. \quad (41)$$

Inserting (39) into (38) and using the relation  $u = \varepsilon\psi$ , we obtain for the nerve impulse the following solution

$$\begin{aligned} u = 2\varepsilon^2 & \left\{ [B_r^{(1)} \cos(\theta) - B_i^{(1)} \sin(\theta)] - \frac{\lambda_1}{\Omega_0^2} [B_r^{(1)2} + B_i^{(1)2}] \right\} \\ & + 2\varepsilon^3 \left\{ [a_1(B_r^{(1)2} - B_i^{(1)2}) + 2a_2B_r^{(1)}B_i^{(1)}] \cos(2\theta) \right. \\ & \left. + [a_2(B_i^{(1)2} - B_r^{(1)2}) + 2a_1B_r^{(1)}B_i^{(1)}] \sin(2\theta) \right\}. \end{aligned} \quad (42)$$

Applying a similar procedure, we obtain for the bursting variable the following initial solution

$$\Phi = 2\varepsilon(B_r^{(2)} \cos \theta - B_i^{(2)} \sin \theta) + \varepsilon^2[C^{(2)} + 2(D_r^{(2)} \cos 2\theta - D_i^{(2)} \sin 2\theta)], \quad (43)$$

where  $B_r^{(2)}$  ( $D_r^{(2)}$ ) and  $B_i^{(2)}$  ( $D_i^{(2)}$ ) are the real and imaginary parts of  $B^{(2)}$  ( $D^{(2)}$ ), respectively. Then we have

$$\begin{aligned} v = \varepsilon\Phi \\ = 2\varepsilon^2(B_r^{(2)} \cos \theta - B_i^{(2)} \sin \theta) + \varepsilon^3[C^{(2)} + 2(D_r^{(2)} \cos 2\theta - D_i^{(2)} \sin 2\theta)], \end{aligned} \quad (44)$$

where

$$B_r^{(2)} = B_i^{(2)} = 0, \quad (45)$$

$$C^{(2)} = -\frac{2d}{e}[B_r^{(1)2} + B_i^{(1)2}], \quad (46)$$

$$D_r^{(2)} = -\frac{d}{e}[B_r^{(1)2} - B_i^{(1)2}], \quad (47)$$

$$D_i^{(2)} = -\frac{2d}{e}[B_r^{(1)} \times B_i^{(1)}]. \quad (48)$$

We also have

$$\beta = 2\varepsilon(B_r^{(3)} \cos \theta - B_i^{(3)} \sin \theta) + \varepsilon^2[C^{(3)} + 2(D_r^{(3)} \cos 2\theta - D_i^{(3)} \sin 2\theta)], \quad (49)$$

where  $B_r^{(3)}$  ( $D_r^{(3)}$ ) and  $B_i^{(3)}$  ( $D_i^{(3)}$ ) are the real and imaginary parts of  $B^{(3)}$  ( $D^{(3)}$ ), respectively. Then we have

$$\begin{aligned} w &= \varepsilon\beta \\ &= 2\varepsilon^2(B_r^{(3)} \cos \theta - B_i^{(3)} \sin \theta) + \varepsilon^3[C^{(3)} + 2(D_r^{(3)} \cos 2\theta - D_i^{(3)} \sin 2\theta)], \end{aligned} \quad (50)$$

where

$$B_r^{(3)}(x, t) = b_1 B_r^{(1)} - b_2 B_i^{(1)}, \quad (51)$$

$$B_i^{(3)}(x, t) = b_1 B_i^{(1)} + b_2 B_r^{(1)}, \quad (52)$$

$$D_r^{(3)}(x, t) = c_{11} D_r^{(1)} - c_2 D_i^{(1)}, \quad (53)$$

$$D_i^{(3)}(x, t) = c_{11} D_i^{(1)} + c_2 D_r^{(1)}, \quad (54)$$

$$C^{(2)}(x, t) = \frac{\Omega_0^2}{r} C^{(1)}, \quad (55)$$

with

$$\begin{aligned} b_1 &= \frac{\Omega_0^2 r}{r^2 + \Omega^2}, & b_2 &= \frac{\Omega_0^2 \Omega}{r^2 + \Omega^2}, \\ c_{11} &= \frac{\Omega_0^2 r}{r^2 + 4\Omega^2}, & \text{and } c_2 &= \frac{2\Omega_0^2 \Omega}{r^2 + 4\Omega^2}. \end{aligned} \quad (56)$$

To have discrete solutions from continuous fractional model (16), we proceed as follows

- We use the initial solution (37) at the points  $\theta = \theta_{n,0} = kx_n$ , where  $x_n = nh$ ,  $1 \leq n \leq M-1$ , and obtain from the linearly implicit Riesz fractional finite-difference scheme the approximated solution  $B_{h,m}^1 \simeq (B^1(x_n, t_m))_{1 \leq n \leq M-1}$ .
- The numerical solution  $B_{h,m}^1$  is now used in (42),(44) and (50) with  $\theta = \theta_{n,m} = kx_n - \Omega t_m$  to obtain the discrete solution  $u_n(t_m) := u(x_n, t_m), v_n(t_m) := v(x_n, t_m)$  and  $w_n(t_m) := w(x_n, t_m)$ .

The discrete solutions  $u_n(t_m), v_n(t_m)$  and  $w_n(t_m)$  obtained from the continuous fractional model (16), can be compared with the numerical solution of (1) from implicit fourth-order Runge-Kutta method. Note that the initial solution used to solve (1) is obtained from (42),(44) and (50) with the same initial solution (37) for  $\theta = \theta_{n,0} = kx_n$ .

In our graphs, the surface plots of  $u_n, v_n$  and  $w_n$  from the continuous fractional model (16) will be called fractional discrete solutions, while the one coming directly from (1) will be called discrete solutions. We should always remember that to have the fractional model (16) the time  $t$ , the coefficients  $\eta_0$ ,  $c_1$  and  $\lambda_3$  have be perturbed at order  $\varepsilon^2$ . So, the fractional discrete solution at time  $t$  will be compared with the discrete solution at time  $\frac{t}{\varepsilon^2}$ .

Figure 4, Figure 5 and Figure 6 show the surface plots of  $u_n, v_n$  and  $w_n$  with different values of  $\varepsilon$ . The fractional graphs of  $u_n$  are those in (a) and the discrete graphs of  $u_n$  are those in (b). The fractional graphs of  $v_n$  are those in (c) and the discrete graphs of  $v_n$  in (d). The fractional graphs of  $w_n$  are those in (e) and discrete graphs of  $w_n$  in (f). All fractional numerical solutions are up to final time  $T = 0.001$ , but in Figure 4 the discrete numerical solutions are up to the final time  $T_f = \frac{T}{\varepsilon^2} = 0.0111$  with  $\varepsilon = 0.2$ . In Figure 5, the discrete numerical solutions are up to the final time  $T_f = \frac{T}{\varepsilon^2} = 0.0111$  with  $\varepsilon = 0.3$ , while in Figure 6, the numerical discrete solutions are up to final time  $T_f = \frac{T}{\varepsilon^2} = 0.0062$  with  $\varepsilon = 0.4$ . From those graphs, we can observe that as the final time  $T_f = \frac{T}{\varepsilon^2}$  decreases, the fractional numerical solutions of  $u_n, v_n$  and  $w_n$  are extremely close to the discrete numerical solutions, therefore the fractional continuous model at (16) and discrete model at (1) are equivalent for relatively small time. The long-range effect therefore mostly contributes to the behavior of the tails of the solutions, as already mentioned.

## 5. Conclusion

The goal of this paper was to study the nonlinear dynamics of a diffusively Hindmarsh-Rose neural network with long-range couplings. Performing a perturbation technique, we have shown that the dynamics of modulated waves in our neural network can be elegantly described by the complex fractional Ginzburg-Landau equation. In general, exact analytical solutions of fractional nonlinear equations cannot be obtained. We have proposed according to the stiffness of the system, the semi implicit Riesz fractional finite-difference scheme and the linearly implicit Riesz fractional finite-difference

scheme to solve efficiently the complex fractional Ginzburg-Landau equation. It has been revealed that the numerical solutions for the nerve impulse are well-localized stable short impulses. The results have been confirmed by the numerical simulations of discrete equations. The work suggests that long-range diffusive couplings could be perceived as a way to transport information via nonlinear waves both in spatial and temporal dimensions for specific processes of the brain to be controlled. The fractional properties observed in our neural network may be also advantageous in excitable systems for crucial intuitions into spatio-temporal dynamics, synchronization and chaos. The work gives also the opportunity to familiarize with improved fractional analytical and numerical methods which can be used to study other systems with long-range couplings.

### **Acknowledgments**

A. Mvogo thanks Dr. habil. Anatole Kenfack of the Institute of Chemistry and Biochemistry, Freie Universitaet Berlin for fruitful discussions. A. Tambue was supported by the Robert Bosch Stiftung within the ARETE chair programme.

### **References**

#### **References**

- [1] Z.P. Kilpatrick and P.C. Bressloff. Stability of bumps in piecewise smooth neural fields with nonlinear adaptation. *Physica D* **239**, 547 (2010).

- [2] D.D. Clarke and L. Sokoloff. Circulation and Energy Metabolism of the Brain. In: G.J. Siegel *et al.* (Eds.) *Basic Neurochemistry: 6th edition, Molecular, Cellular and Medical Aspects*, Lippincott-Raven, Philadelphia, 1999.
- [3] F.M. Moukam Kakmeni, E.M. Inack, E.M. Yamakou. Localized nonlinear excitations in diffusive Hindmarsh-Rose neural networks. *Phys. Rev. E* **89**, 052919 (2014).
- [4] S.R. Dtchetgnia Djeundam, R. Yamapi, G. Filatrella, T.C. Kofane, Stability of the synchronized network of Hindmarsh-Rose neuronal models with nearest and global couplings. *Commun. Nonlinear Sci. Numer. Simul.* **22**, 545-563 (2015).
- [5] E. Steur, I. Tyukin, H. Nijmeijer, Semi-passivity and synchronization of diffusively coupled neuronal oscillators. *Physica D*, **238**, 2119 (2009).
- [6] B.N. Lundstrom, A.L. Fairhall, M. Maravall. Multiple time scale encoding of slowly varying whisker stimulus envelope in cortical and thalamic neurons in vivo. *J. Neuroscience* **30**, 50715077, (2010).
- [7] B.N. Lundstrom, M.H. Higgs, W.J. Spain, A.L. Fairhall. Fractional differentiation by neocortical pyramidal neurons. *Nature Neuroscience* **11**, 13351342, (2008).
- [8] S. Shen, F. Liu, V. Anh, I. Turner, J. Chen. A novel numerical approximation for the space fractional advection-dispersion equation. *IMA Journal of Applied Mathematics*, **79**, 431-444 (2014).

- [9] J.L. Hindmarsh and R.M. Rose. A model of neuronal bursting using three coupled first order differential equations. *Proc. R. Soc. London, Ser. B* **221**, 87-102 (1984).
- [10] R. Fitzhugh. Impulses and physiological states in theoretical models of nerve membrane. *Biophys. J.* **1**, 445-466 (1961).
- [11] V.V. Zosimov and R.M. Lyamsshev, Fractals in wave processes *Usp. Fiz. Nauk* **165**, 361-402 (1995).
- [12] A. Mvogo, G.H. Ben-Bolie, T.C. Kofane. Coupled fractional nonlinear differential equations and exact Jacobian elliptic solutions for exciton phonon dynamics. *Phys. Lett. A* **378**, 2509 (2014).
- [13] A. Mvogo, G.H. Ben-Bolie, T.C. Kofane. Energy transport in the three coupled  $\alpha$ -polypeptide chains of collagen molecule with long-range interactions effect. *Chaos* **25**, 063115 (2015).
- [14] V.E. Tarasov and G.M. Zaslavsky. Fractional dynamics of systems with long-range interaction. *Commun. Nonlinear Sci. Numer. Simul.* **11**, 885-898 (2006).
- [15] V.E. Tarasov and G.M. Zaslavsky. Fractional Ginzburg-Landau equation for fractal media. *Physica A*, **354**, 249261 (2005).
- [16] N. Laskin and G.M. Zaslavsky. Nonlinear fractional dynamics on a lattice with longrange interactions. *Physica A* **368**, 3814 (2006).
- [17] S.G. Samko, A.A. Kilbas, O.I. Marichev. *Fractional Integrals and*

- Derivatives Theory and Applications. *Gordon and Breach, New York*, 1993.
- [18] H. Weitzner and G.M. Zaslavsky. Some applications of fractional derivatives. *Commun. Nonlinear Sci. Numer. Simul.* **8**, 273 (2003).
- [19] A.V. Milovanov, J.J. Rasmussen. Fractional generalization of the Ginzburg-Landau equation: an unconventional approach to critical phenomena in complex media. *Phys. Lett. A* **337**, 75 (2005).
- [20] C.D. Negro, C.-F. Hsiao, S. Chandler, A. Garfinkel. Evidence for a novel bursting mechanism in rodent trigeminal neurons. *BioPhys. J.* **75**, 174-182 (1998).
- [21] C.M. Pedroarena *et al.*. Oscillatory membrane potential activity in the soma of a primary afferent neuron. *J. Neurophysiology* **82**(1465) (1999).
- [22] A.K. Al Azad and P. Ashwin. Within-burst synchrony changes for coupled elliptic bursters. *SIAM J. Appl. Dyn. Syst.* **9**, 261 (2010).
- [23] A. Tambue, Efficient Numerical schemes for Porous Media Flow. *PhD thesis, Department of Mathematics, Heriot-Watt University*, 2010.
- [24] A. Tambue, G.J. Lord, S. Geiger. An exponential integrator for advection-dominated reactive transport in heterogeneous porous media. *Journal of Computational Physics* , **229**(10), 3957-3969 (2010).
- [25] A. Tambue, S. Geiger and G.J. Lord. Exponential Time integrators for 3D Reservoir Simulation. *In proceedings of the 12th European Conference on the Mathematics of Oil Recovery, Oxford, UK*, 2010.

- [26] K. Nozaki and N. Bekki. Exact Solutions of the Generalized Ginzburg-Landau Equation. *J. Phys. Soc. Jpn.* **53**, 1581-1582 (1984).
- [27] N.R. Pereira and L. Stenflo. Nonlinear Schrödinger equation including growth and damping. *Phys. Fluids* **20**, 1733-1734 (1977).
- [28] A.M. Dikande and G.A. Bartholomew. Localized short impulses in a nerve model with self-excitable membrane. *Phys. Rev. E*, **80**, 041904 (2009).
- [29] A. Tambue, I. Berre and J. M. Nordbotten. Efficient simulation of geothermal processes in heterogeneous porous media based on the exponential Rosenbrock-Euler and Rosenbrock-type methods. *Advances in Water Resources* , **53**, 250-262 (2013).
- [30] C. Celik, and M. Duman. Crank–Nicolson method for the fractional diffusion equation with the Riesz fractional derivative. *Journal of Computational Physics*, 231 (2012) 1743–1750.

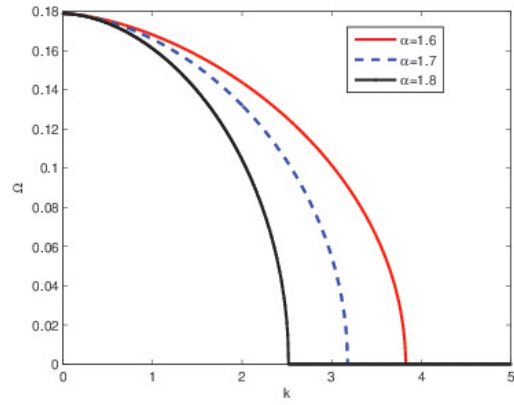
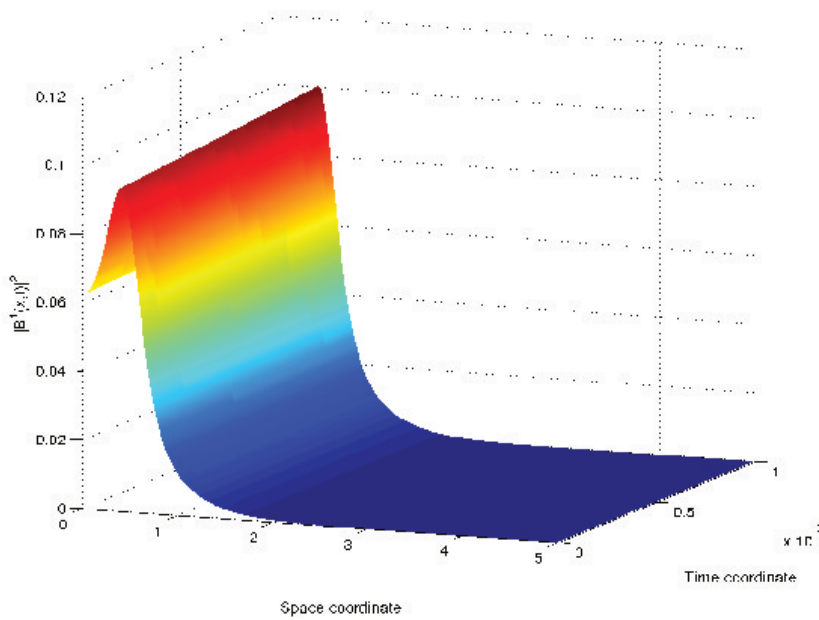


Figure 1: The dispersion relation of the nerve impulse according to three different values of  $\alpha$ , namely  $\alpha = 1.6$ ,  $\alpha = 1.7$  and  $\alpha = 1.8$ .  $\Omega_0^2 = 0.032$  and  $c_0 = 0.001$ . It appears that the long-rang parameter  $\alpha$  affects the dispersion area.



(a)

Figure 2: (Color online) Profile of the numerical solution  $|B^1(x,t)|^2$  according to time and space for  $\alpha = 1.8$  at up to the final time  $T = 0.001$ .

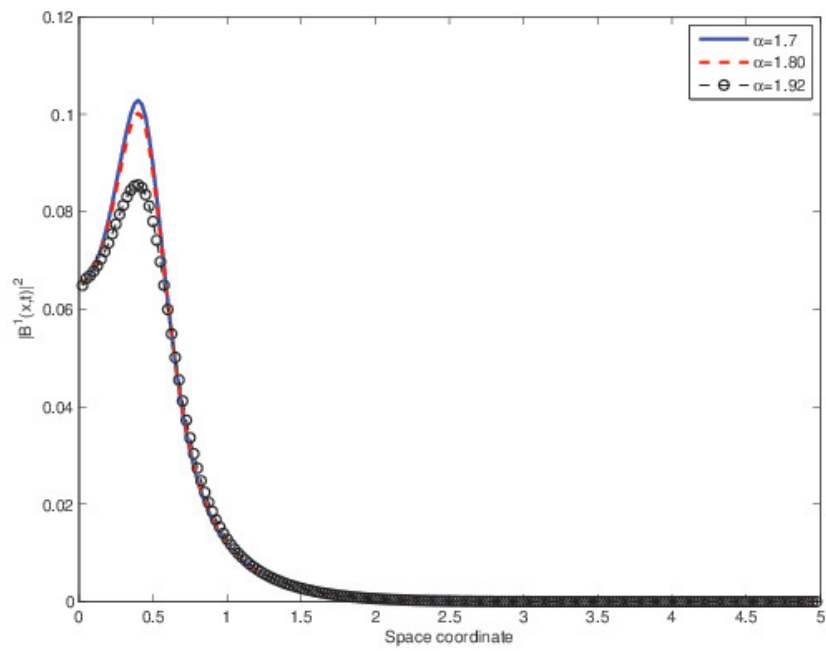
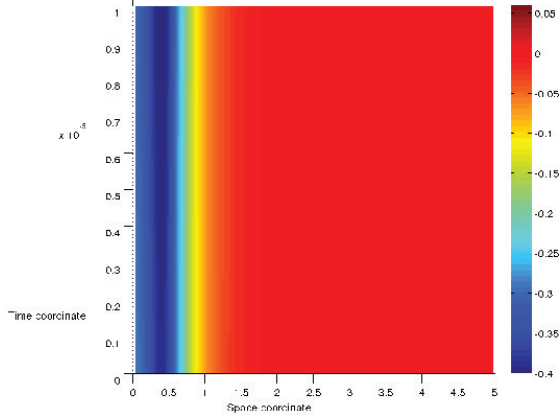
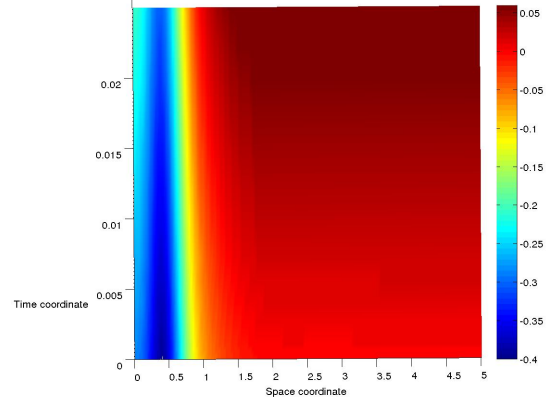


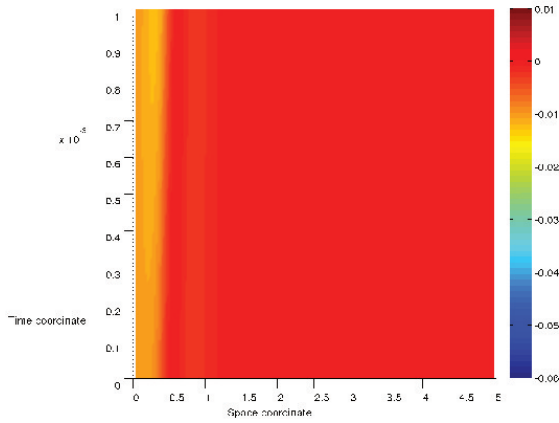
Figure 3: Spatial profile of the numerical solution  $|B^1(x, t)|^2$  at time  $t = 0.001$  with initial nonlinear localized solution with  $\alpha = 1.7$ ,  $\alpha = 1.8$ , and  $\alpha = 1.92$ .



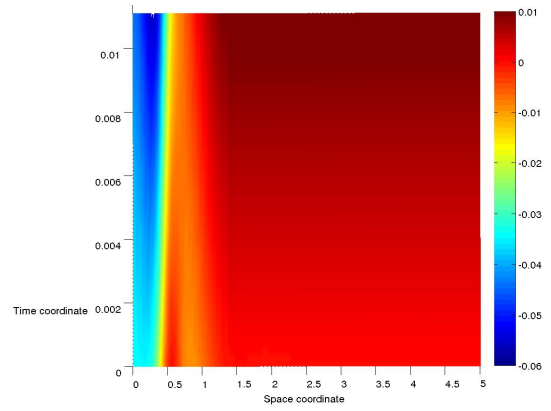
(a)



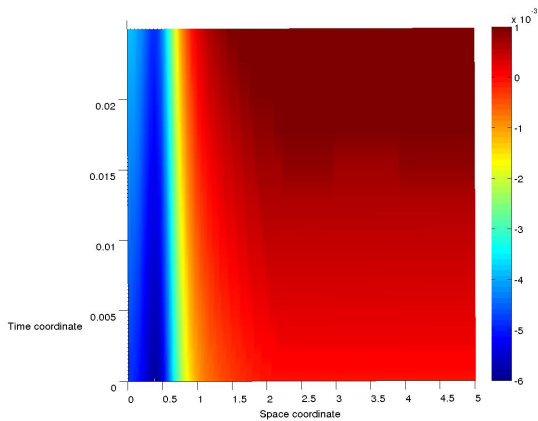
(b)



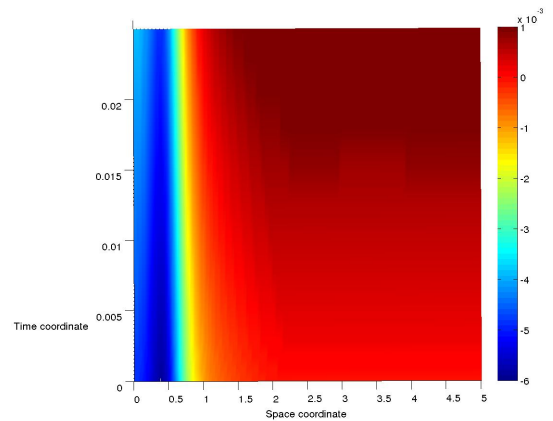
(c)



(d)

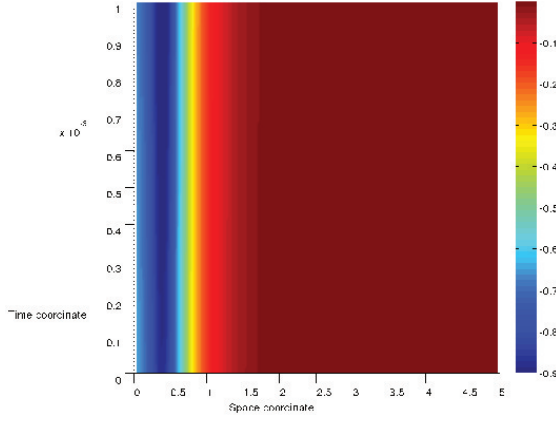


(e)

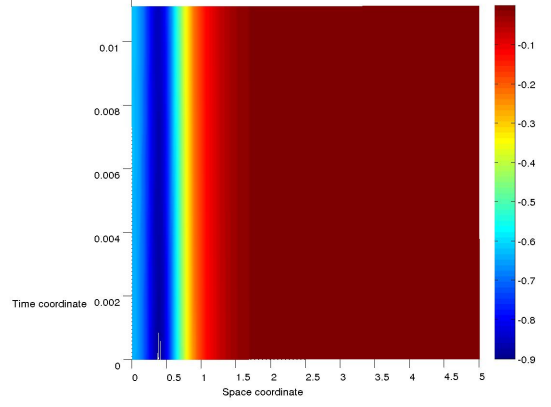


(f)

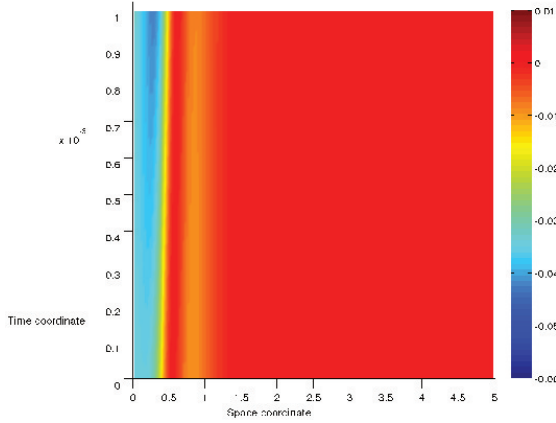
Figure 4: Fractional  $u_n$  (a) and discrete  $u_n$ (b), fractional  $v_n$  (c) and discrete  $v_n$  (d), and fractional  $w_n$  (e) and discrete  $w_n$  (f). The fractional solutions are up to final time  $T = 0.001$  while the discrete solutions are up to the final time  $T_f = \frac{T}{\varepsilon^2} = 0.025$  with  $\varepsilon = 0.2$



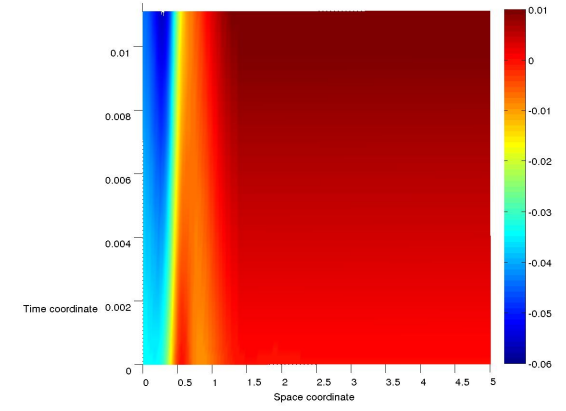
(a)



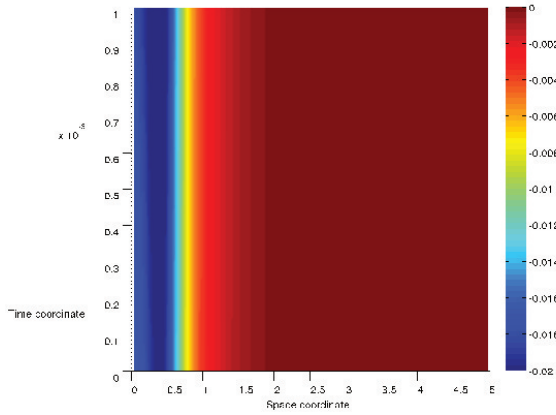
(b)



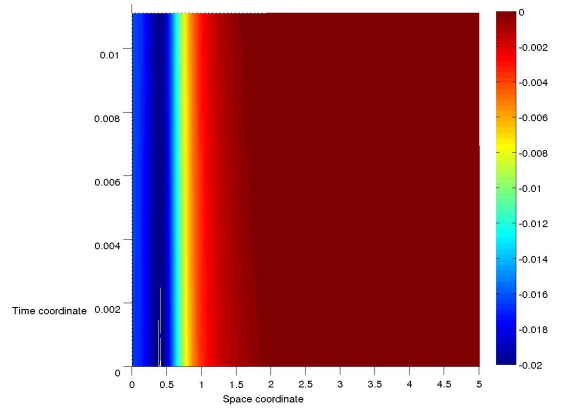
(c)



(d)

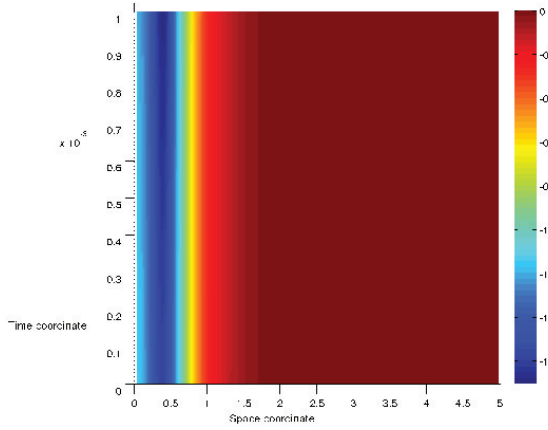


(e)

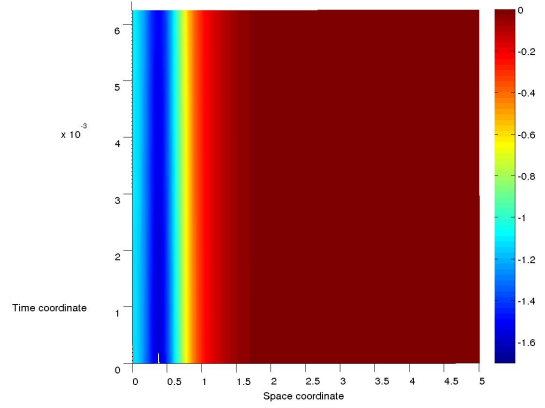


(f)

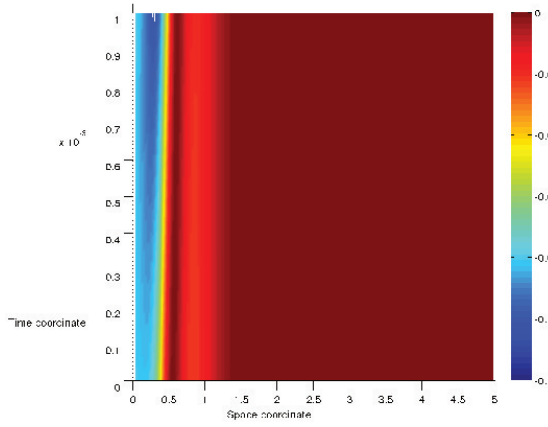
Figure 5: Fractional  $u_n$  (a) and discrete  $u_n$  (b), fractional  $v_n$  (c) and discrete  $v_n$  (d), and Fractional  $w_n$  (e) and discrete  $w_n$  (f). The fractional solutions are up to final time  $T = 0.001$  while the discrete solutions are up to the final time  $T_f = \frac{T}{\varepsilon^2} = 0.0111$  with  $\varepsilon = 0.3$ .



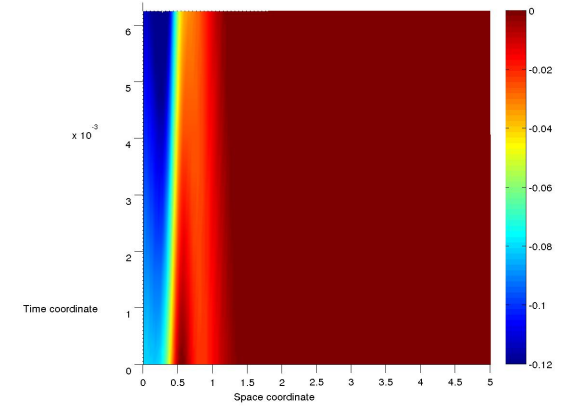
(a)



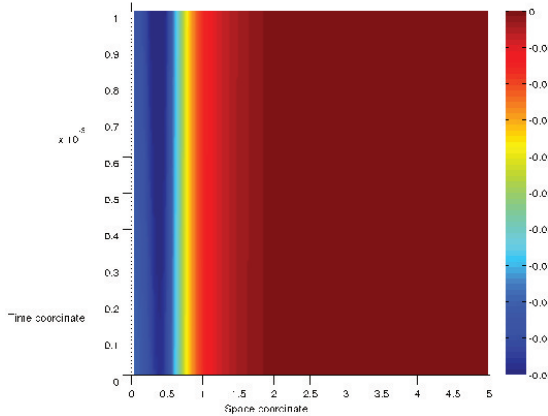
(b)



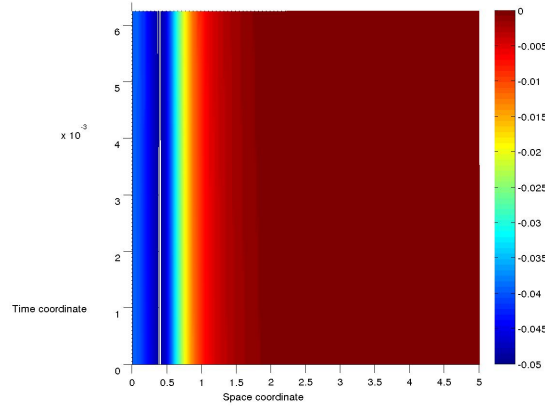
(c)



(d)



(e)



(f)

Figure 6: Fractional  $u_n$  (a) and discrete  $u_n$ (b), fractional  $v_n$  (c) and discrete  $v_n$  (d), and fractional  $w_n$  (e) and discrete  $w_n$  (f). The fractional solutions are up to final time  $T = 0.001$  while the discrete solutions are up to the final time  $T_f = \frac{T}{\varepsilon^2} = 0.0062$  with  $\varepsilon = 0.4$ .